NANO LETTERS

Letter

pubs.acs.org/NanoLett

Low-Frequency Interlayer Breathing Modes in Few-Layer Black Phosphorus

Xi Ling,*[†,¶] Liangbo Liang,[‡,¶] Shengxi Huang,[†] Alexander A. Puretzky,[§] David B. Geohegan,[§] Bobby G. Sumpter,[§,∥] Jing Kong,[†] Vincent Meunier,*[‡] and Mildred S. Dresselhaus*[†,⊥]

[†]Department of Electrical Engineering and Computer Science, Massachusetts Institute of Technology, Cambridge, Massachusetts 02139, United States

[‡]Department of Physics, Applied Physics, and Astronomy, Rensselaer Polytechnic Institute, Troy, New York 12180, United States

[§]Center for Nanophase Materials Sciences, Oak Ridge National Laboratory, Oak Ridge, Tennessee 37831, United States

[∥]Computer Science and Mathematics Division, Oak Ridge National Laboratory, Oak Ridge, Tennessee 37831, United States

[⊥]Department of Physics, Massachusetts Institute of Technology, Cambridge, Massachusetts 02139, United States

Supporting Information

ABSTRACT: As a new two-dimensional layered material, black phosphorus (BP) is a very promising material for nanoelectronics and optoelectronics. We use Raman spectroscopy and first-principles theory to characterize and understand the low-frequency (LF) interlayer breathing modes (<100 cm^{-1}) in few-layer BP for the first time. Using a laser polarization dependence study and group theory analysis, the breathing modes are assigned to A_g symmetry. Compared to the high-frequency (HF) Raman modes, the LF breathing modes are considerably more sensitive to interlayer coupling and, thus, their frequencies show a stronger dependence on the number of layers. Hence, they constitute an effective means to probe both the crystalline orientation and thickness of few-layer BP. Furthermore, the temperature dependence shows that in the temperature range −150 to 30 °C, the breathing modes have a weak anharmonic behavior, in contrast to the HF Raman modes that exhibit strong anharmonicity.

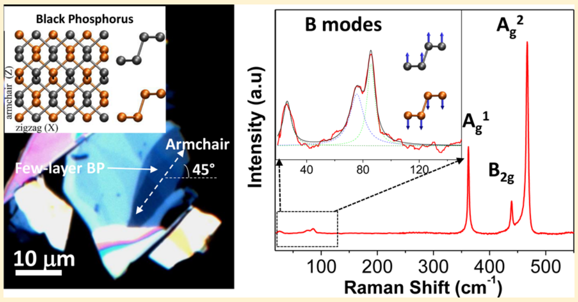

KEYWORDS: *Raman spectroscopy, polarization dependence, thickness dependence, temperature dependence, density functional theory*

Orthorhombic black phosphorus (BP) is the most stable allotrope of phosphorus. It features a layered structure with puckered monolayers stacked by van der Waals (vdW) forces.[1] Few- or single-layer BP can be mechanically exfoliated from bulk BP.[2−5] Due to BP's intrinsic thickness-dependent direct bandgap (ranging from 0.3 eV for bulk to 2.0 eV for a monolayer) and relatively high carrier mobility (up to ∼1000 $cm^2\ V^{-1}\ s^{-1}$ at room temperature),[2,4,6−9] it is expected to have promising applications in nanoelectronic devices[2−4,10] and for near and mid-infrared photodetectors.[11−19] Recently, high performance thermoelectric devices were also predicted based on BP thin films.[20−22] With the surge of interest in two-dimensional (2D) materials (such as graphene and transition metal dichalcogenides (TMDs)),[23,24] BP has become a "hot material" because it bridges the bandgap between graphene and TMDs and offers the best trade-off between mobility and on−off ratio.[3] Moreover, the unique anisotropic puckered honeycomb lattice of BP leads to many novel in-plane anisotropic properties, which could lead to even more applications.[3,9,25,26]

Phonons play an important role in the diverse properties of materials,[27] and they have been intensively studied in vdW layered materials, such as graphene and TMDs.[28−35] Raman spectroscopy is a nondestructive particularly powerful tool to investigate phonons and their coupling to electrons, and it has been successfully applied to vdW layered materials.[36−40] Due to the lattice dynamics of vdW layered materials, the phonon modes can be classified as high-frequency (HF) intralayer modes and low-frequency (LF) interlayer modes.[27] Intralayer modes involve vibrations from the intralayer chemical bonds (Figure 1c), and their associated frequencies reflect the strength of those bonds. In contrast, the interlayer modes correspond to layer−layer vibrations with each layer vibrating as a whole unit (Figure 1b), and hence, their frequencies are determined by the interlayer vdW restoring forces. The weak nature of vdW interactions typically renders the frequencies of interlayer modes much lower than those of intralayer modes, usually below 100 cm^{-1}. Depending on the vibrational direction, LF interlayer modes are categorized into two types: the in-plane shear modes and the out-of-plane breathing modes (Figure 1b). Due to their greater sensitivity to interlayer coupling, the LF interlayer modes have been shown to be very important in identifying the thickness for few-layer graphite and TMDs.[41−43]

Received: March 22, 2015
Revised: April 27, 2015
Published: May 8, 2015

DOI: 10.1021/acs.nanolett.5b01117
Nano Lett. 2015, 15, 4080−4088

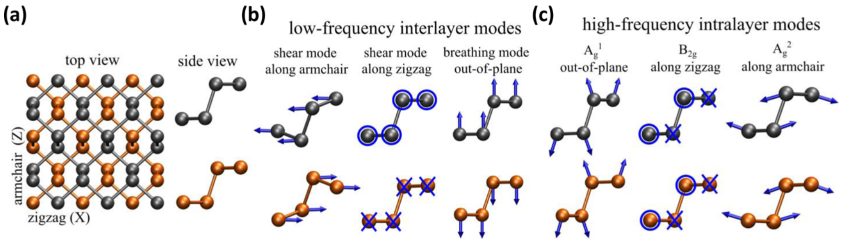

Figure 1. (a) Top and side views of BP with puckered layers. The top and bottom layers are differentiated using black and gold colors, respectively. (b) Vibrations of LF interlayer modes: two in-plane shear modes and one out-of-plane breathing mode. (c) Vibrations of HF intralayer modes: three characteristic Raman modes A_g^1, B_{2g}, and A_g^2. The circle and cross indicate vibrations coming out of the plane of the page and going into it, respectively.

The HF intralayer Raman modes in bulk BP crystals were studied in the 1980s[44] and recently similar HF modes have been reported in thin film BP.[3,45–47] Normally, three characteristic HF Raman modes (A_g^1, B_{2g}, and A_g^2) can be observed under the typical backscattering configuration, corresponding to the out-of-plane vibration (~365 cm^{-1}), in-plane vibrations along the zigzag (~440 cm^{-1}) and armchair (~470 cm^{-1}) directions, respectively (Figure 1c). Moreover, it is found that their dependence on the laser polarization can be used to determine the crystalline orientation of BP.[45,47] However, the frequencies of the HF intralayer modes are found to exhibit almost no dependence on film thickness.[44–47] Clearly, study of the LF interlayer phonon modes in few-layer BP (Figure 1b) is needed to reveal more information on the interlayer coupling and thickness. LF phonons have been studied in bulk BP using inelastic neutron scattering in the 1980s.[48,49] However, to the best of our knowledge, there has been no experimental work on the observation of LF interlayer modes in few-layer BP and only two theoretical works have been published recently.[50,51] The measurement of LF (<100 cm^{-1}) Raman modes is challenging because these modes are usually blocked by the notch filters used to reject the excitation laser light, and the LF measurements require a Raman system with a LF rejection filter or a triple-grating Raman system. In this work, we successfully observed the LF interlayer breathing Raman modes in few-layer BP for the first time. These breathing modes are assigned to A_g symmetry and can be also used for crystalline orientation determination according to an experimental laser polarization dependence analysis and first-principles density functional theory (DFT) calculations. The thickness dependence study indicates that the breathing modes in few-layer BP are strongly thickness-dependent and, thus, could be used as an important and effective indicator of the number of layers. In addition, based on our temperature dependence study, the breathing modes show much smaller anharmonic shifts compared to those observed for HF modes.

According to symmetry analysis,[52,53] the bulk BP crystal belongs to the space group *Cmce* (No. 64) and point group D_{2h}^{18} (*mmm*).[44] Note that the space group is labeled as *Cmca* (No. 64) in the old convention of the International Tables of Crystallography. As shown in Figure 1a, the crystal unit cell of bulk BP is orthorhombic with two layers and 8 atoms (a = ~3.3 Å, b = ~10.5 Å, and c = ~4.4 Å). The primitive unit cell is half of the crystal unit cell and contains four atoms, and hence there are 12 normal phonon modes at the Γ point

$$\Gamma_{\text{bulk}} = 2A_g + B_{1g} + B_{2g} + 2B_{3g} + A_u + 2B_{1u} + 2B_{2u} + B_{3u} \qquad (1)$$

where the A_g, B_{1g}, B_{2g}, B_{3g} modes are Raman-active, the B_{1u}, B_{2u}, B_{3u} modes are infrared-active, and the A_u mode is optically inactive.[44,45,54] According to the classical Placzek approximation,[55] the Raman intensity of a phonon mode is proportional to $|e_i \cdot \tilde{R} \cdot e_s^T|^2$, where e_i and e_s are the electric polarization vectors of the incident and scattered light, respectively, and $\tilde{R}$ is the Raman tensor of the phonon mode. Only when $|e_i \cdot \tilde{R} \cdot e_s^T|^2$ is not zero, can the phonon mode be observed by Raman spectroscopy. As a common practice in the literature,[44,45,53] we denote the in-plane zigzag direction as the x axis, the out-of-plane direction as the y axis, and in-plane armchair direction as the z axis. The calculated Raman tensors $\tilde{R}$ of Raman-active modes A_g, B_{1g}, B_{2g}, and B_{3g} are

$$\tilde{R}(A_g) = \begin{pmatrix} a & \cdot & \cdot \\ \cdot & b & \cdot \\ \cdot & \cdot & c \end{pmatrix} \quad \tilde{R}(B_{1g}) = \begin{pmatrix} \cdot & d & \cdot \\ d & \cdot & \cdot \\ \cdot & \cdot & \cdot \end{pmatrix}$$
$$\tilde{R}(B_{2g}) = \begin{pmatrix} \cdot & \cdot & e \\ \cdot & \cdot & \cdot \\ e & \cdot & \cdot \end{pmatrix} \quad \tilde{R}(B_{3g}) = \begin{pmatrix} \cdot & \cdot & \cdot \\ \cdot & \cdot & f \\ \cdot & f & \cdot \end{pmatrix} \qquad (2)$$

where a–f are major terms while other terms (denoted by "·") are either zero or negligible due to symmetry.[45,56,57] In the typical experimental backscattering configuration, the electric polarization vectors e_i and e_s are in-plane (the X–Z plane), and thus only A_g and B_{2g} modes can be observed according to the Raman tensors, although B_{1g} and B_{3g} are Raman-active (more details are provided in Supporting Information).[42,45–47] The symmetries of *N-layer* (*NL*) BP films (where N is the number of layers) are slightly different from those of bulk BP: odd *NL* BP belongs to space group *Pmna* (No. 53) and point group D_{2h}^{7} (*mmm*); even *NL* BP belongs to space group *Pmca* (No. 57) and point group D_{2h}^{11} (*mmm*). Although *NL* systems belong to different space groups from the bulk BP, all of them share the same point group D_{2h} (*mmm*). Consequently, the symmetry classification of Raman modes and the forms of their Raman tensors remain unchanged for any thickness (eqs 1 and 2), consistent with previous theoretical works.[51,57,58]

In *NL* BP, there are $N - 1$ interlayer shear modes vibrating along the zigzag direction, $N - 1$ interlayer shear modes along the armchair direction, and $N - 1$ interlayer breathing modes along the out-of-plane direction, similar to 2D graphene and TMDs.[41,43,50] The difference is that the shear modes vibrating along zigzag and armchair directions are nondegenerate in BP due to its in-plane anisotropy. For perfect (defect-free and free-standing) BP films, the shear modes are either Raman-active (B_{1g} or B_{3g}) or infrared-active (B_{1u} or B_{3u}). Similarly, the breathing modes are either Raman-active (A_g) or infrared-active

Table 1. Calculated Frequencies, in cm^{-1}, of the Breathing Modes for 2L to 8L BP Using the DFT PBE+optB88 Method[a]

Layer number	B1	B2	B3	B4	B5	B6	B7
2	62.7						
3	52.0	70.5					
4	36.2	63.1	75.6				
5	33.7	53.4	69.5	76.2			
6	31.9	42.1	55.1	71.0	78.6		
7	28.2	35.7	51.7	65.2	74.5	80.4	
8	24.8	31.0	47.8	60.9	71.4	77.6	83.2
bulk							86.1

[a] In *NL* BP, there are $N - 1$ breathing modes either Raman-active (A_g, highlighted in red) or infrared-active (B_{2u}, in black). The number of breathing modes with Raman-active A_g symmetry is $N/2$ for even N, and $(N - 1)/2$ for odd N. The breathing modes are labeled as B*n*. The breathing mode of bulk BP is also shown but it cannot be detected.

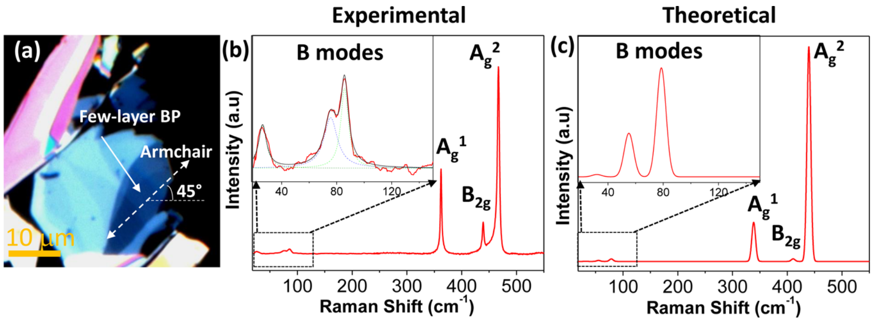

Figure 2. (a) Typical optical image of exfoliated BP flakes on a glass substrate coated with parylene, including few-layer BP (the blue area). The armchair direction is labeled, determined by the polarization dependence study. (b) Experimental Raman spectrum of few-layer BP corresponding to the flake in (a). Inset: the zoom-in spectrum from 20 to 150 cm^{-1}, the dotted lineshapes show the three fitted Lorentzian B modes. (c) Calculated Raman spectrum of 6L BP in the experimental backscattering geometry. Inset: the zoom-in spectrum in the same LF region as (b). Three interlayer breathing modes (B modes) with Raman-active A_g symmetry are predicted in the LF range. In (c), the HF A_g^1 and A_g^2 peaks are reduced in intensity by ~50 times for comparison purposes.

(B_{2u}).[51] As shown by in eq 2, in the backscattering configuration, only A_g and B_{2g} modes can be detected by Raman spectroscopy. Consequently, among the LF interlayer modes, only the Raman-active breathing modes with A_g symmetry can be observed in the Raman spectra. Furthermore, the number of breathing modes with Raman-active A_g symmetry is $N/2$ for even *NL* and $(N - 1)/2$ for odd *NL* (see Table 1).[51] For monolayer BP (or phosphorene), the interlayer breathing modes do not exist. Bulk BP has a breathing mode (around 87 cm^{-1}),[48−50,54] but its calculated Raman tensor $\tilde{R}$ is zero, indicating that it cannot be detected. Therefore, in short, the breathing modes can only be observed in few-layer BP, not in single-layer and bulk BP. In addition, according to the inelastic neutron scattering measurements on bulk BP,[48−50,54] the two shear modes (vibrating along armchair and zigzag directions, respectively) have frequencies around 19 and 52 cm^{-1}, whereas the frequency is ~87 cm^{-1} for the breathing mode. From our calculations and previous theoretical works,[50,51] in few-layer BP, the frequencies of all shear modes are no larger than their bulk values (thus, $\leq$52 cm^{-1}); similarly the frequencies of all breathing modes are no larger than their bulk values (thus, $\leq$87 cm^{-1}). These results suggest that LF peaks observed above 52 cm^{-1} likely originate from the breathing modes.

The experimental Raman measurements were carried out on few-layer BP flakes (Figure 2). The BP flakes deposited on a glass substrate were mechanically exfoliated from the bulk and coated with a parylene (~100 nm) or PMMA film (~300 nm) immediately to avoid sample degradation. From the optical contrast of the flakes, the bluish flakes are determined as few-layer BP, whereas the reddish and whitish flakes are thicker ones.[2,3,59] The corresponding Raman spectrum on the few-layer BP (the blue area labeled in Figure 2a) is shown in Figure 2b. The three well-known HF A_g^1, B_{2g}, and A_g^2 peaks of BP are located at 362.3 cm^{-1}, 439.2 cm^{-1}, and 467.1 cm^{-1}, respectively.[3] More interestingly, another three peaks with relatively weaker intensities are observed in the LF region. As shown in the zoom-in spectrum in the inset of Figure 2b, the frequencies of these three peaks are determined by peak fitting as 26.2 cm^{-1}, 75.6 cm^{-1}, and 85.6 cm^{-1}, respectively. According to our theoretical analysis, they are expected to be LF interlayer breathing modes (labeled as "B modes") belonging to Raman-active A_g symmetry. In addition, only when $N \geq 6$ can there be no less than three B modes with A_g symmetry. Therefore, we conclude that the number of layers of the measured few-layer BP flake in Figure 2a is at least 6. The calculated Raman spectrum of 6L BP is shown in Figure 2c. Besides the A_g^1, B_{2g}, and A_g^2 modes in the HF region, three B modes appear in the LF region, with their frequencies located around 31.9 cm^{-1},

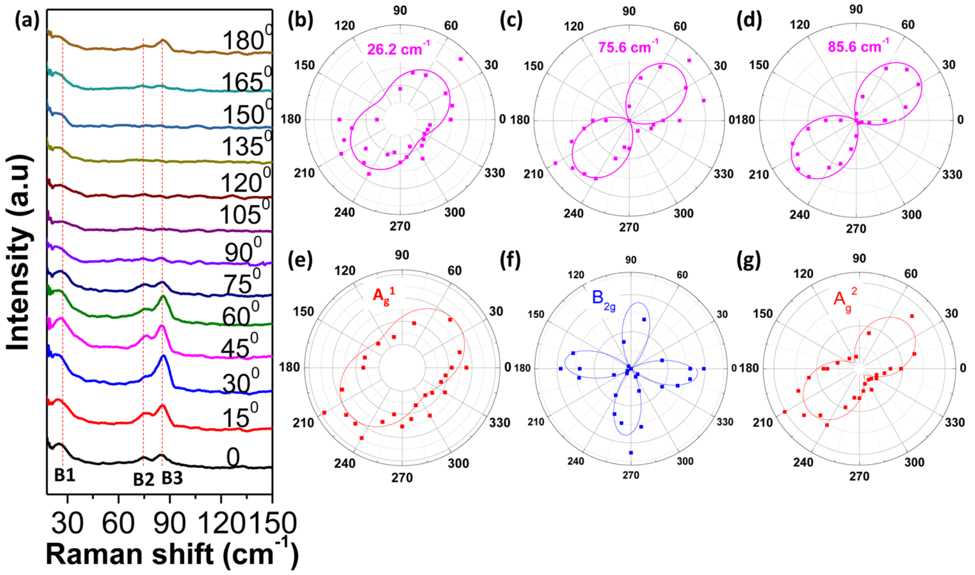

Figure 3. (a) Raman spectra of few-layer BP in the LF range at different sample rotation angles. (b–d) The profiles of the intensities of the LF interlayer breathing modes at different rotation angles: (b) 26.2 cm^{-1}; (c) 75.6 cm^{-1}; (d) 85.6 cm^{-1}. (e–g) Profiles of the intensities of the HF intralayer modes at different rotation angles. (e) A_g^1; (f) B_{2g}; (g) A_g^2. The sample was rotated clockwise from 0° to 360°.

55.1 cm^{-1}, and 78.6 cm^{-1} (inset in Figure 2c), confirming our interpretation of the experimental observations. To provide further experimental evidence that the three LF Raman peaks in Figure 2b are B modes with A_g symmetry, we performed laser polarization dependence measurements of all Raman modes, as shown in the following.

Due to the in-plane anisotropic structure of the BP thin film, its Raman modes show a significant polarization dependence, which can be used to identify the crystalline orientation of the sample.[45,47] Two methods were reported to study the polarization dependence. One is by rotating the sample while fixing the polarization of the incident and scattered light;[45] the other is by changing the polarization of the incident and scattered light while fixing the sample.[47] Here, we employed the first method. As discussed above, the Raman intensity has the relation as $I \propto |e_i \cdot \tilde{R} \cdot e_s^T|^2$ In the experimental backscattering geometry, the electric polarization vectors e_i and e_s of the incident and scattered light are in-plane (the X–Z plane: X (Z) axis is defined as the sample initial zigzag (armchair) direction before rotating the sample). By setting the polarization angle of the incident (scattered) light as θ (γ) with respect to the X axis, we have

$$I \propto \left| (\cos\theta,\ 0,\ \sin\theta)\tilde{R}\begin{pmatrix}\cos\gamma\\ 0\\ \sin\gamma\end{pmatrix} \right|^2$$

In our case, θ and γ are fixed, and the sample is rotated in the X–Z plane by φ with respect to X axis. The Raman intensity then becomes

$$I \propto \left| (\cos(\theta-\varphi),\ 0,\ \sin(\theta-\varphi))\tilde{R}\begin{pmatrix}\cos(\gamma-\varphi)\\ 0\\ \sin(\gamma-\varphi)\end{pmatrix} \right|^2$$

(more details are provided in the Supporting Information).

In our experiment, we used the parallel polarization configuration, so that $\gamma = \theta$ always. For an A_g mode, its Raman tensor is

$$\tilde{R} = \begin{pmatrix} a & \cdot & \cdot\\ \cdot & b & \cdot\\ \cdot & \cdot & c\end{pmatrix}$$

and thus

$$I_{A_g} \propto a^2\left|1 + \left(\frac{c}{a} - 1\right)\sin^2(\varphi - \theta)\right|^2 \tag{3}$$

Because θ is fixed, the intensity of an A_g mode depends on both the sample rotation angle φ and the ratio c/a. For a B_{2g} mode, the Raman tensor is

$$\tilde{R} = \begin{pmatrix} \cdot & \cdot & e\\ \cdot & \cdot & \cdot\\ e & \cdot & \cdot\end{pmatrix}$$

and thus

$$I_{B_{2g}} \propto e^2\sin^2 2(\varphi - \theta) \tag{4}$$

which only depends on the rotation angle φ, since θ is fixed. According to our calculations and a previous experimental work for few-layer BP,[45] c (tensor component related to the armchair direction) is expected to be larger than a (tensor component related to the zigzag direction) in eq 3, and hence $c/a > 1$. Therefore, the minimum intensity angle of an A_g mode is $\varphi = \theta$ or θ + 180° (the sample zigzag direction is now rotated to the polarization direction of the incident light); the maximum intensity angle of an A_g mode is $\varphi = \theta + 90°$ or $\theta + 270°$ (the sample armchair direction is now rotated to the polarization direction of the incident light). The minimum intensity angle of a B_{2g} mode is $\varphi = \theta$, $\theta + 90°$, $\theta + 180°$, or $\theta + 270°$ (the sample's armchair or zigzag direction is now rotated to be aligned with the polarization direction of the incident light); its maximum intensity angle is $\varphi = \theta + 45°$, $\theta + 135°$, $\theta + 225°$, or $\theta + 315°$. Hence, by rotating the sample under a parallel polarization configuration, the intensity variation period is always 180° for an A_g mode, whereas it is 90° for a B_{2g} mode. In addition, when the sample armchair (zigzag) direction is along the polarization direction of the incident light, an A_g mode shows the maximum (minimum) intensity, whereas a B_{2g} mode is forbidden.[45] These simple results can be used as effective indicators of the crystalline orientation.

Note that the above theoretical analysis is based on real Raman tensor elements, while strictly speaking they should be complex.[60] This leads to no change for the polarization dependence of a B_{2g} mode, but a phase difference between the complex Raman tensor elements *a* and *c* is introduced and certain values of the phase difference can result in two maximum intensity peaks for an A_g mode.[45,60] One peak corresponds to the sample armchair direction and the other corresponds to the sample zigzag direction. The main effect of the phase difference is to induce a minimum intensity peak between the armchair and zigzag directions.[60] By varying the phase difference, the overall polarization dependence profile of an A_g mode will be changed.[45,60] Nevertheless, for any value of the phase difference, we found that the intensities and angles of the maximum and secondary maximum intensity peaks do not change (intensities are always $|c|^2$ and $|a|^2$, whereas angles always correspond to armchair and zigzag directions). Therefore, the angle of the maximum intensity peak of an A_g mode always corresponds to the same crystalline orientation, independent of the phase difference. Hence the most important result from the polarization dependence study holds even when the Raman tensor elements are complex. Moreover, as discussed in Figure 3 for our BP sample, the phase difference is assumed to have such a value that no secondary maximum intensity peak appears for any A_g mode (where the minimum intensity peak actually appears), and thus, the effect of the complex Raman tensor and phase difference is insignificant in our work.

Figure 3a shows a series of Raman spectra of few-layer BP in the LF region at different sample rotation angles. The corresponding Raman spectra in the HF region are shown in Supporting Information Figure S3. With the sample rotated from 0° to 180°, the intensities of the three LF modes vary periodically, and reach maximum and minimum values around 45° and 135°, respectively. It should be mentioned that we could not differentiate the LF modes from the background noise for the rotation from 105° to 165° because the associated peaks are too weak at these polarization values. These results clearly establish the importance of considering the sample orientation relative to the polarization of the incident light when studying the LF modes of BP. The polar plots of the fitted peak intensities of both the LF and HF modes as a function of the rotation angle are shown in Figures 3b−g. The three LF modes (Figure 3b−d) and HF A_g^1 and A_g^2 modes (Figure 3e and g) share a very similar polarization dependence: all of them have the same intensity variation period of 180° with two intensity maxima around 45° or 225°. However, the HF B_{2g} mode shows the intensity variation period of 90° with four intensity maxima around 0°, 90°, 180°, 270° (Figure 3f). These are consistent with our theoretical predictions discussed above and the theoretical polar plots in Supporting Information Figure S2. The polarization dependence measurement further confirms that the three LF modes share the same symmetry as the HF A_g^1 and A_g^2 modes (i.e., A_g symmetry). These three LF modes, thus, are assigned to interlayer breathing modes that have A_g symmetry, because shear modes (belonging to B_{1g} or B_{3g} symmetry)[51] have a different polarization dependence from the A_g modes. Note that although the LF breathing (B) modes and the HF A_g modes share a very similar polarization dependence in Figures 3b−g, there are still minor differences. At the minimum intensity rotation angles (~135° or 315°), one notes that the LF B mode (26.2 cm^{-1}) and HF A_g^1 and A_g^2 modes show relatively strong intensities, whereas the LF B modes (75.6 and 85.6 cm^{-1}) are barely present. This can be explained by different values of the *c*/*a* ratio in the Raman tensors of the B and A_g modes despite the existence of an identical symmetry (see eq 3 and Supporting Information Figure S2a).

In addition, the polarization dependence study further indicates that the armchair direction of the sample is oriented about the 45° direction shown in Figure 2a because the maximum intensity angles of the B and A_g modes correspond to the sample armchair direction (see additional details in the Supporting Information). It is important to point out that our combined experimental/theoretical analysis is based on the assumption that the ratio $c/a > 1$, which is consistent with a previous experimental work.[45] In the present work, for few-layer BP under the 632.8 nm laser excitation wavelength, it is expected that $c/a > 1$. However, an increase in BP thickness (to a very thick sample) and a change in laser wavelength (toward Raman resonance) could modify the *c*/*a* ratio and possibly to values smaller than 1, as reported by some authors recently.[60] If $c/a < 1$, for an A_g mode, the intensity variation period is still 180°, but the maximum intensity angle corresponds to the zigzag direction instead of the armchair direction. Regardless of the *c*/*a* ratio being larger or smaller than 1, it is certain that the intensity angle extrema correspond to the armchair or zigzag direction.[45,60]

As suggested by the polarization dependence, the intensities of the Raman modes of BP are strongly related to the crystalline orientations relative to the polarization of the incident light. Therefore, when studying the thickness dependence of the Raman modes, it is important to set the flakes along the same crystalline orientation. Therefore, for every flake chosen for a thickness dependence study, we collected the Raman spectra of the flakes at different orientations and determined the armchair direction of each of the flakes. The B modes of the different flakes are all collected with the laser polarization along the armchair direction, at which orientation the intensities reach the maximum. The optical images and the corresponding Raman spectra of the flakes on 300 nm SiO_2/Si substrates with a PMMA coating are shown in Figure 4. Because the BP sample is polymer coated immediately after exfoliation to avoid degradation, it becomes very difficult to directly measure the thicknesses of the flakes using, for example, atomic force microscopy (AFM). But from the optical contrast of the flakes, their relative thicknesses can be determined to order from the thinnest flake to the thickest one marked as 1 and 5, respectively (Figure 4a). On flake 1, we did not observe any LF peak at any polarization direction (Figure 4b). In addition, the Raman intensities of the HF modes on flake 1 are very weak (Figure S4 in Supporting Information). These results indicate that flake 1 is likely a monolayer (recall that a monolayer cannot have LF interlayer modes).[12,46,61] For the few-layer BP in Figure 4b, from flake 2 to flake 3, a LF B mode appears and the Raman peak splits into two from flake 4 to flake 5. However, for very thick multilayer (ML) flakes and bulk samples, the LF B mode is not observed (Figure 4b). The absence of the LF modes in bulk BP is consistent with the theoretical analysis outlined above. For very

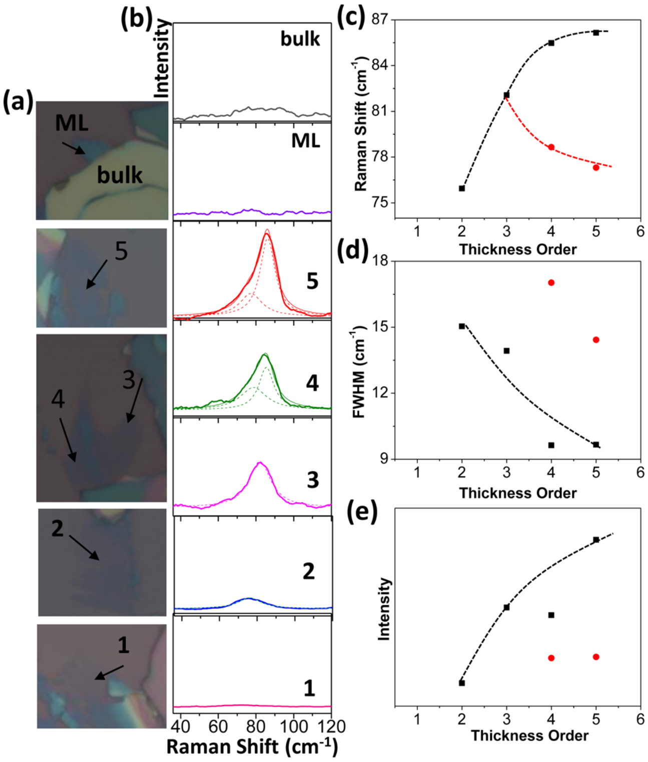

Figure 4. (a) Optical images of BP flakes with different thicknesses. The thickness increases with the flake from bottom to top. (b) Raman spectra collected on the flakes corresponding to (a) in the LF range. The dash lines are the Lorentzian peak fittings. (c–e) Raman shift (c), fwhm line widths (d), and intensities (e) of the breathing modes as a function of the thickness. The black (red) points correspond to the higher-frequency (lower-frequency) breathing modes.

thick ML flakes that are bulk-like, the intensities of LF modes are too low to be detected. It is only in the few-layer samples (flakes 2–5 in Figure 4b) that the LF modes show observable intensities. Such a tendency is consistent with other vdW layered materials such as TMDs, where bulk-inactive vibrational modes become Raman-active and observable in few-layer flakes, but they are nondetectable in very thick samples.[41,62,63] In addition, we also show the dependence of the full-width half-maximum (fwhm) (Figure 4d) and intensity (Figure 4e) of the B modes on thickness. The decrease of the fwhm with the increase of the flake thickness indicates that the lifetime of the B mode phonons is longer in the thicker flakes, similar to TMDs.[64] In Figure 4e, the intensity of the higher-frequency B mode generally increases with the flake thickness from flake 2 to 5.

To understand the thickness dependence of the B modes, we calculated the frequencies of B modes of 2L to 8L BP using the DFT PBE+optB88 method (Table 1). This method gives the bulk B mode's frequency 86.1 cm^{-1}, which is very close to the experimental value (87 cm^{-1}).[48−50,54] Other DFT functionals have also been used for comparison (more details are provided in Table S1 in Supporting Information). In each column of Table 1, the frequency of the B mode monotonically decreases with increasing flake thickness, consistent with previous theoretical works on BP[50,51] and experimental reports on TMDs,[40,41] as this constitutes a general trend for vdW layered materials. Furthermore, the highest-frequency B mode of any thickness BP in Table 1 is the bulk-like B mode, where each adjacent layer is vibrating in opposite directions (see the vibrations in Supporting Information Figure S1). With increasing thickness, the highest-frequency B mode blue shifts and approaches the bulk limit of 87 cm^{-1}, very similar to that observed for the higher-frequency B mode (the black points in Figure 4c). It follows that the observed higher-frequency mode in a BP flake should correspond to the flake's highest-frequency B mode (i.e., bulk-like B mode). As for the lower-frequency B mode (the red points in Figure 4c), it probably corresponds to the second-highest B mode of the flake. Note that only these two B modes can be unambiguously observed for BP flakes 2–5. The other Raman-active B modes predicted in Table 1 are too difficult to be detected experimentally, possibly due to their weak intensities or too low frequencies. Similarly, only two B modes can be observed in few-layer TMDs as well.[42] Because the highest-frequency B mode is not Raman-active (B_{2u}) for odd N, the BP flakes 2–5 showing bulk-like B modes might be all even *NL*. Another possibility is that the polymer capping or the supporting substrates or defects in the material may break the symmetry to induce Raman-activation of the bulk-like B modes in odd *NL* BP. A definite conclusion cannot be drawn because direct measurements of the flakes' thickness cannot be performed in this experiment because it requires protection capping of the unstable BP with a polymer. Nevertheless, we showed in Figure 4c that the frequency changes of the LF B modes with increasing thickness can exceed 10 cm^{-1}, whereas the frequency variations of the HF A_g^1, B_{2g}, and A_g^2 modes are much smaller (∼2 cm^{-1}, see Supporting Information Figure S4).[44−47,61] Consequently, the LF modes could offer an effective approach to determine the flake thickness and probe the interlayer vdW coupling of BP after the corresponding calibration measurements. We expect that the present work can stimulate further experimental efforts to identify the thickness and probe the LF modes, thus establishing more conclusive relationships between them.

The temperature dependence of the Raman spectra is important for understanding the fine structure and properties of the material, by probing phonons and their interactions with other particles, which in turn is expected to have a large impact on the performance of BP-based electronic and thermoelectric devices. The temperature dependence of the B, A_g^1, B_{2g}, and A_g^2 modes of the BP flake in Figure 2 is measured under 632 nm laser excitation from −150 to 30 °C (Figure 5 and Supporting Information Figure S5). The data are fitted using a linear temperature dependent equation:[65] $\omega = \omega_0 + \chi T$ (red lines in Figure 5), where ω_0 is the frequency at $T = 0$ °C and χ is the first-order temperature coefficient, which defines the slope of the dependence. It can be clearly seen that the different modes have different temperature dependences. In particular, the B mode shows a very weak temperature dependence, which has almost no frequency change in the examined temperature range (Figure 5a) with $\omega_B = 87.4 - 1.8 \times 10^{-4} T$ for -150 °C $< T < 30$ °C. This suggests a very weak anharmonic property of the B mode in few-layer BP.[65,66] However, anharmonic phonon effects occur for the HF modes according to the stronger temperature dependence (Figures 5b–d), where $\omega_{Ag1} = 361 - 0.0073T$ for A_g^1, $\omega_{B2g} = 438 - 0.013T$ for B_{2g}, and $\omega_{Ag2} = 465 - 0.012T$ for A_g^2, all for -150 °C $< T < 30$ °C. Furthermore, the first-order temperature coefficient is larger for the in-plane vibrational modes (B_{2g} and A_g^2) than for the out-of-plane vibrational mode (A_g^1). This is consistent with the results obtained for bulk BP.[56] The temperature coefficients of the in-plane Raman modes of few-layer BP (−0.013 cm^{-1}/K for the B_{2g} mode and −0.012 cm^{-1}/K for the A_g^2 mode) are similar to

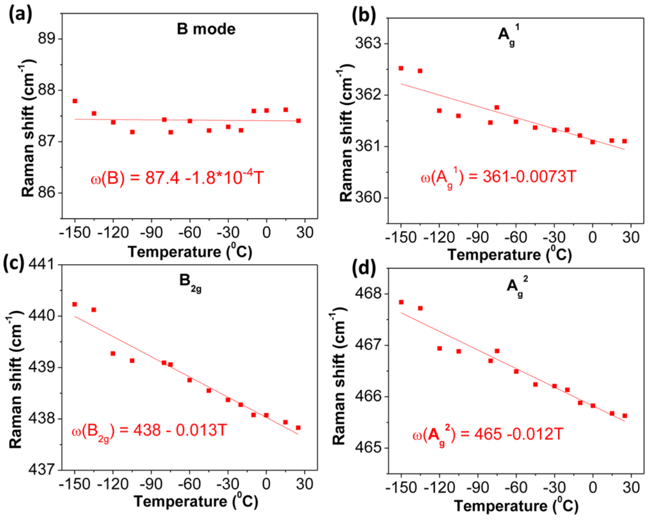

Figure 5. Temperature dependence of the frequencies of the breathing mode (a), A_g^1 (b), B_{2g} (c), and A_g^2 (d) modes. The red lines are the corresponding fitting lines.

some other layered materials, such as graphene (−0.015 cm^{-1}/K for the G band)[66,67] and MoS$_2$ (−0.013 cm^{-1}/K for the E_{2g} mode).[68,69]

In Figure 5, we fitted the data linearly and considered the first-order temperature coefficient χ, which has two components leading to the Raman frequency shift. The temperature dependence of the Raman frequency can be rewritten as $\omega = \omega_0 + \chi_T\Delta T + \chi_V\Delta T = \omega_0 + (\partial\omega/\partial T)_V\,\Delta T + (\partial\omega/\partial V)_T\Delta V$, where the first term $(\partial\omega/\partial T)_V\Delta T$ is the "self-energy" shift, which is the pure temperature effect, and the second term $(\partial\omega/\partial V)_T\Delta V$ is due to the crystal thermal expansion.[65,66] For the out-of-plane B mode of few-layer BP, which is solely due to interlayer coupling, the contribution to the Raman shift from the second term $(\partial\omega/\partial V)_T\Delta V$ depends on the thermal expansion along the out-of-plane direction. Because the interlayer distance does not change appreciably with temperature, the thermal expansion along the out-of-plane direction can be ignored.[70,71] Therefore, the contribution from the crystal thermal expansion can be ignored for the B mode, as confirmed by our calculations (Supporting Information Figure S6a). Thus, the weak anharmonic behavior of the B mode in the temperature range −150 to 30 °C in Figure 5a suggests that the contribution from the first term $((\partial\omega/\partial T)_V\Delta T)$ should be near zero as well, indicating the weak phonon coupling for the B mode. For the HF out-of-plane intralayer mode A_g^1, the contribution from the in-plane thermal expansion is also negligible (supported by the calculation results shown in Supporting Information Figure S6b). Hence, the anharmonic behavior of the A_g^1 mode in Figure 5b is largely due to the "self-energy shift" (i.e., the anharmonic phonon coupling). However, for the HF in-plane intralayer modes B_{2g} and A_g^2, the contribution from the in-plane thermal expansion is significant (as revealed by the calculations shown in Supporting Information Figure S6c−d) because the tensile stress can be induced in the BP plane and the sequential softening of the P−P bonds occurs with increasing temperature. The anharmonic phonon effect for the B_{2g} and A_g^2 modes in Figure 5c−d, thus, is mainly due to the decrease of the force constants by the thermal expansion.

In conclusion, the determination of the thickness and crystalline orientation are two crucial aspects for advancing studies of few-layer BP. Raman spectroscopy is expected to provide considerable insight into both aspects due to this nondestructive and convenient characterization method. The identification of the crystalline orientation has been successfully achieved using the polarization dependence of the HF intralayer Raman modes.[45,47] However, these modes fail to provide information on BP's thickness. In this work, for the first time, the LF interlayer breathing modes are observed in few-layer BP and show promising potential for identifying both the crystalline orientation and the thickness, as well as probing the interlayer vdW coupling. The breathing modes are assigned to the same symmetry as the HF A_g modes, since they share a similar laser polarization dependence. By rotating the few-layer sample under a parallel polarization configuration using the 632.8 nm laser excitation wavelength, they all show the same intensity variation period of 180° with the strongest intensities occurring when the sample armchair direction is along the polarization direction of the light. The crucial difference is that the LF breathing modes are found to be much more sensitive to the thickness and interlayer interactions, compared to the HF Raman modes. Furthermore, the temperature dependence study shows that in the temperature range −150 to 30 °C, the breathing mode has very small anharmonicity, whereas the HF modes show large anharmonic shifts, suggesting different phonon−phonon coupling behaviors among LF and HF modes. Overall, these experimental/theoretical results on BP phonons, especially the low-frequency phonons, should be very helpful for future studies of the electronic and thermal properties of BP thin films.

Methods. *Sample Preparation.* Few-layer BP was prepared on a 300 nm SiO$_2$/Si substrate or glass substrate by mechanical exfoliation from a bulk BP and coated immediately by parylene (~100 nm) or PMMA film (~300 nm) immediately to avoid the degradation of BP. The locations of the flakes are identified under an optical microscope.

Raman Measurements. The Raman spectra in Figures 2−4 were recorded under a backscattering configuration at room temperature on a triple-grating Horiba-Yobin T64000 micro-Raman system with a 632.8 nm He−Ne laser line, 1800 lines/mm grating, a micrometer resolved XYZ scanning stage, and a 100× objective lens of NA = 0.95. The laser spot diameter is about 1 μm on the sample and the laser power is controlled at around 2.5 mW. For the polarization dependence measurement, the sample was placed on a rotation stage. The sample was rotated during the measurement every 10−15°, and the polarization of the incident light and scattered light was kept parallel. The Raman spectra in Figure 5 for the temperature dependence study was carried out on a Horiba Jobin Yvon HR800 system with a 632.8 nm He−Ne laser line, 600 lines/mm grating, a micrometer resolved XYZ scanning stage, and a × 100 objective lens of NA = 0.80. The laser power is around 1 mW on the sample. The temperature was controlled by a Linkam thermal stage THMS 600. The parameters of the Raman peaks are obtained by fitting the peaks using a Lorentzian line shape. We chose a 632.8 nm (1.96 eV) excitation laser in this work instead of 532.5 nm (2.33 eV) laser to avoid the photolysis of BP under the high energy laser, since the bonding energy of the P−P bond is around 2.1 eV.

Theoretical Methods. Plane-wave DFT calculations were performed using the VASP package equipped with projector augmented wave (PAW) pseudopotentials for electron−ion interactions.[72,73] Previous theoretical calculations have demonstrated that the geometrical and electronic properties of bulk and few-layer BP are highly functional dependent.[25,74] Therefore, for comparison and completeness, the exchange-correlation interactions are considered in the local density approximation (LDA), as well as the generalized gradient approximation (GGA) using the Perdew−Burke−Ernzerhof (PBE) functional.[75] For the GGA-PBE calculations, vdW interactions between layered BP are included using the DFT-D2 approach of Grimme (denoted as PBE+D2),[76] and the vdW density functional methods optB88-vdW (denoted as PBE+optB88) and optB86b-vdW (denoted as PBE+optB86b).[77] For bulk BP, both atoms and cell volume were allowed to relax until the residual forces were below 0.001 eV/Å, with a cutoff energy set at 500 eV and a 12 × 4 × 9 *k*-point sampling in the Monkhorst−Pack scheme.[78] By taking the in-plane zigzag direction as the X axis, the out-of-plane direction as the Y axis, and in-plane armchair direction as the Z axis, the optimized lattice parameters of bulk BP are $a = 3.35$ Å, $b = 10.67$ Å, and $c = 4.45$ Å using optB88-vdW. Single- and few-layer BP systems were then modeled by a periodic slab geometry using the optimized in-plane lattice constant of the bulk. A vacuum region of 22 Å in the direction normal to the plane (Y direction) was used to avoid spurious interactions with replicas. For the 2D slab calculations, all atoms were relaxed until the residual forces were below 0.001 eV/Å and 12 × 1 × 9 k-point samplings were used.

Nonresonant Raman calculations were performed using the fully relaxed geometries. Because the Raman intensity is given by $I \propto |e_\mathrm{i} \cdot \tilde{R} \cdot e_\mathrm{s}^\mathrm{T}|$,[2] the calculations of the Raman tensors $\tilde{R}$ are of the most importance, which requires the information on the phonon frequencies, phonon eigenvectors (i.e., vibrations), and the changes of the polarizability or the dielectric constant tensors with respect to phonon vibrations (see more details and equations in ref 55). To obtain Raman scattering, one needs to calculate the dynamic matrix and derivatives of the dielectric constant tensors. The dynamic matrix was calculated using the finite difference scheme and implemented in the Phonopy software.[52,79] Hellmann−Feynman forces in the 3 × 1 × 3 supercell were computed by VASP for both positive and negative atomic displacements ($\delta = 0.03$ Å) and were then used in Phonopy to construct the dynamic matrix, whose diagonalization provides phonon frequencies and eigenvectors. Phonopy was also used to determine the space and point groups of a system, and the symmetry of each phonon mode. The derivatives of the dielectric constant tensors were also calculated by the finite difference approach. For both positive and negative atomic displacements in the single unit cell, the dielectric constant tensors were computed by VASP using density functional perturbation theory and then their derivatives can be obtained. With phonon frequencies, phonon eigenvectors and derivatives of the dielectric constant tensors, the Raman tensors $\tilde{R}$ can then be computed. From this, the Raman intensity for every phonon mode is obtained for a given laser polarization setup to finally yield a Raman spectrum after Gaussian broadening.

■ ASSOCIATED CONTENT

Ⓢ Supporting Information

Thickness-dependent interlayer breathing modes in BP; polarization dependence of Raman-active modes in BP; high-frequency Raman spectra at different crystal rotation angles; thickness dependence of the high-frequency Raman modes; temperature dependence of the Raman modes. The Supporting Information is available free of charge on the ACS Publications website at DOI: 10.1021/acs.nanolett.5b01117.

■ AUTHOR INFORMATION

Corresponding Authors

*E-mail: mdress@mit.edu. Tel.: +1-617-253-6864.
*E-mail: meuniv@rpi.edu. Tel.: +1-518-276-6886.
*E-mail: xiling@mit.edu. Tel.: +1-617-253-6860.

Author Contributions

¶These authors contributed equally to this work.

Author Contributions

X.L., S.H., J.K., and M.S.D. initiated the project and designed the experiments. X.L., S.H., and A.A.P. performed experimental measurements and analyzed the data. L.L. and V.M. performed the theoretical analysis. X.L., L.L., S.H., V.M., and M.S.D. wrote the paper. All authors discussed the results and commented on the manuscript.

Notes

The authors declare no competing financial interest.

■ ACKNOWLEDGMENTS

The authors thank Prof. Fengnian Xia, Prof. Han Wang, Sangyeop Lee, and Weihua Mu for their useful discussion and help. X.L., S.H., and M.S.D. at MIT acknowledge grant DE-SC0001299 for financial support. Part of the Raman measurements was conducted at the Center for Nanophase Materials Sciences, which is sponsored at Oak Ridge National Laboratory by the Scientific User Facilities Division, Office of Basic Energy Sciences, U.S. Department of Energy. The theoretical work at Rensselaer Polytechnic Institute (RPI) was supported by New York State under NYSTAR program C080117 and the Office of Naval Research. The computations were performed using the resources of the Center for Computational Innovation at RPI.

■ REFERENCES

(1) Morita, A. *Appl. Phys. Solids Surf.* **1986**, *39* (4), 227−242.

(2) Li, L.; Yu, Y.; Ye, G. J.; Ge, Q.; Ou, X.; Wu, H.; Feng, D.; Chen, X. H.; Zhang, Y. *Nat. Nanotechnol.* **2014**, *9* (5), 372−377.

(3) Xia, F.; Wang, H.; Jia, Y. *Nat. Commun.* **2014**, *5*, 4458.

(4) Liu, H.; Neal, A. T.; Zhu, Z.; Luo, Z.; Xu, X.; Tománek, D.; Ye, P. D. *ACS Nano* **2014**, *8* (4), 4033−4041.

(5) Koenig, S. P.; Doganov, R. A.; Schmidt, H.; Neto, A. H. C.; Özyilmaz, B. *Appl. Phys. Lett.* **2014**, *104* (10), 103106.

(6) Rodin, A. S.; Carvalho, A.; Castro Neto, A. H. *Phys. Rev. Lett.* **2014**, *112* (17), 176801.

(7) Asahina, H.; Morita, A. *J. Phys. C: Solid State Phys.* **1984**, *17* (11), 1839−1852.

(8) Liang, L.; Wang, J.; Lin, W.; Sumpter, B. G.; Meunier, V.; Pan, M. *Nano Lett.* **2014**, *14* (11), 6400−6406.

(9) Tran, V.; Soklaski, R.; Liang, Y.; Yang, L. *Phys. Rev. B* **2014**, *89* (23), 235319.

(10) Wang, H.; Wang, X.; Xia, F.; Wang, L.; Jiang, H.; Xia, Q.; Chin, M. L.; Dubey, M.; Han, S. *Nano Lett.* **2014**, *14* (11), 6424−6429.

(11) Buscema, M.; Groenendijk, D. J.; Blanter, S. I.; Steele, G. A.; van der Zant, H. S. J.; Castellanos-Gomez, A. *Nano Lett.* **2014**, *14* (6), 3347−3352.

(12) Wang, X.; Jones, A. M.; Seyler, K. L.; Tran, V.; Jia, Y.; Zhao, H.; Wang, H.; Yang, L.; Xu, X.; Xia, F. Highly Anisotropic and Robust Excitons in Monolayer Black Phosphorus. 2014, *arXiv:1411.1695v1*. arXiv.org e-Print archive. http://arxiv.org/abs/1411.1695 (accessed April 2015).

(13) Low, T.; Roldán, R.; Wang, H.; Xia, F.; Avouris, P.; Moreno, L. M.; Guinea, F. *Phys. Rev. Lett.* **2014**, *113* (10), 106802.

(14) Engel, M.; Steiner, M.; Avouris, P. *Nano Lett.* **2014**, *14* (11), 6414−6417.

(15) Buscema, M.; Groenendijk, D. J.; Steele, G. A.; van der Zant, H. S. J.; Castellanos-Gomez, A. *Nat. Commun.* **2014**, *5*, 4651.

(16) Liu, H.; Du, Y.; Deng, Y.; Ye, P. D. *Chem. Soc. Rev.* **2015**, *44*, 2732−2743.
(17) Churchill, H. O. H.; Jarillo-Herrero, P. *Nat. Nanotechnol.* **2014**, *9* (5), 330−331.
(18) Xia, F.; Wang, H.; Xiao, D.; Dubey, M.; Ramasubramaniam, A. *Nat. Photonics* **2014**, *8*, 899−907.
(19) Ling, X.; Wang, H.; Huang, S.; Xia, F.; Dresselhaus, M. S. *Proc. Natl. Acad. Sci. U.S.A.* **2015**, *112* (15), 4523−4530.
(20) Qin, G.; Yan, Q.-B.; Qin, Z.; Yue, S.-Y.; Cui, H.-J.; Zheng, Q.-R.; Su, G. *Sci. Rep.* **2014**, *4*, 6946.
(21) Fei, R.; Faghaninia, A.; Soklaski, R.; Yan, J.-A.; Lo, C.; Yang, L. *Nano Lett.* **2014**, *14* (11), 6393−6399.
(22) Lv, H. Y.; Lu, W. J.; Shao, D. F.; Sun, Y. P. Large thermoelectric power factors in black phosphorus and phosphorene. 2014, *arXiv:1404.5171*. arXiv.org e-Print archive. http://arxiv.org/abs/1404.5171 (accessed April 2015).
(23) Geim, A. K.; Novoselov, K. S. *Nat. Mater.* **2007**, *6* (3), 183−191.
(24) Wang, Q. H.; Kalantar-Zadeh, K.; Kis, A.; Coleman, J. N.; Strano, M. S. *Nat. Nanotechnol.* **2012**, *7* (11), 699−712.
(25) Qiao, J.; Kong, X.; Hu, Z.-X.; Yang, F.; Ji, W. *Nat. Commun.* **2014**, *5*, 4475.
(26) Fei, R.; Yang, L. *Nano Lett.* **2014**, *14* (5), 2884−2889.
(27) Zabel, H. *J. Phys.: Condens. Matter* **2001**, *13* (34), 7679.
(28) Chen, J.-H.; Jang, C.; Xiao, S.; Ishigami, M.; Fuhrer, M. S. *Nat. Nanotechnol.* **2008**, *3* (4), 206−209.
(29) Hwang, E. H.; Das Sarma, S. *Phys. Rev. B* **2008**, *77* (11), 115449.
(30) Efetov, D. K.; Kim, P. *Phys. Rev. Lett.* **2010**, *105* (25), 256805.
(31) Bonini, N.; Lazzeri, M.; Marzari, N.; Mauri, F. *Phys. Rev. Lett.* **2007**, *99* (17), 176802.
(32) Lui, C. H.; Malard, L. M.; Kim, S.; Lantz, G.; Laverge, F. E.; Saito, R.; Heinz, T. F. *Nano Lett.* **2012**, *12* (11), 5539−5544.
(33) Uchida, S.; Tanaka, S. *J. Phys. Soc. Jpn.* **1978**, *45* (1), 153−161.
(34) Stirling, W. G.; Dorner, B.; Cheeke, J. D. N.; Revelli, J. *Solid State Commun.* **1976**, *18* (7), 931−933.
(35) Li, H.; Zhang, Q.; Yap, C. C. R.; Tay, B. K.; Edwin, T. H. T.; Olivier, A.; Baillargeat, D. *Adv. Funct. Mater.* **2012**, *22* (7), 1385−1390.
(36) Ferrari, A. C. *Solid State Commun.* **2007**, *143* (1−2), 47−57.
(37) Yan, J.; Zhang, Y.; Kim, P.; Pinczuk, A. *Phys. Rev. Lett.* **2007**, *98* (16), 166802.
(38) Chakraborty, B.; Bera, A.; Muthu, D. V. S.; Bhowmick, S.; Waghmare, U. V.; Sood, A. K. *Phys. Rev. B* **2012**, *85* (16), 161403.
(39) Lee, C.; Yan, H.; Brus, L. E.; Heinz, T. F.; Hone, J.; Ryu, S. *ACS Nano* **2010**, *4* (5), 2695−2700.
(40) Ferrari, A. C.; Basko, D. M. *Nat. Nanotechnol.* **2013**, *8* (4), 235−246.
(41) Zhang, X.; Han, W. P.; Wu, J. B.; Milana, S.; Lu, Y.; Li, Q. Q.; Ferrari, A. C.; Tan, P. H. *Phys. Rev. B* **2013**, *87* (11), 115413.
(42) Zhao, Y.; Luo, X.; Li, H.; Zhang, J.; Araujo, P. T.; Gan, C. K.; Wu, J.; Zhang, H.; Quek, S. Y.; Dresselhaus, M. S.; Xiong, Q. *Nano Lett.* **2013**, *13* (3), 1007−1015.
(43) Lui, C. H.; Heinz, T. F. *Phys. Rev. B* **2013**, *87* (12), 121404.
(44) Sugai, S.; Shirotani, I. *Solid State Commun.* **1985**, *53* (9), 753−755.
(45) Wu, J.; Mao, N.; Xie, L.; Xu, H.; Zhang, J. *Angew. Chem.* **2015**, *127* (8), 2396−2399.
(46) Castellanos-Gomez, A.; Vicarelli, L.; Prada, E.; Island, J. O.; Narasimha-Acharya, K. L.; Blanter, S. I.; Groenendijk, D. J.; Buscema, M.; Steele, G. A.; Alvarez, J. V.; Zandbergen, H. W.; Palacios, J. J.; van der Zant, H. S. J. *2D Mater.* **2014**, *1* (2), 025001.
(47) Zhang, S.; Yang, J.; Xu, R.; Wang, F.; Li, W.; Ghufran, M.; Zhang, Y.-W.; Yu, Z.; Zhang, G.; Qin, Q.; Lu, Y. *ACS Nano* **2014**, *8* (9), 9590−9596.
(48) Fujii, Y.; Akahama, Y.; Endo, S.; Narita, S.; Yamada, Y.; Shirane, G. *Solid State Commun.* **1982**, *44* (5), 579−582.
(49) Yamada, Y.; Fujii, Y.; Akahama, Y.; Endo, S.; Narita, S.; Axe, J.; McWhan, D. *Phys. Rev. B* **1984**, *30* (5), 2410−2413.
(50) Jiang, J.-W.; Wang, B.-S.; Park, H. S. Interlayer Breathing and Shear Modes in Few-Layer Black Phosphorus. 2014, *arXiv:1412.7587*. arXiv.org e-Print archive. http://arxiv.org/abs/1412.7587 (accessed June 2014).
(51) Cai, Y.; Ke, Q.; Zhang, G.; Feng, Y. P.; Shenoy, V. B.; Zhang, Y.-W. *Adv. Funct. Mater.* **2015**, online.
(52) Togo, A.; Oba, F.; Tanaka, I. *Phys. Rev. B* **2008**, *78* (13), 134106.
(53) Aroyo, M. I.; Perez-Mato, J. M.; Orobengoa, D.; Tasci, E.; de la Flor, G.; Kirov, A. *Bulg. Chem. Commun.* **2011**, *43* (2), 183−197.
(54) Kaneta, C.; Katayama-Yoshida, H.; Morita, A. *J. Phys. Soc. Jpn.* **1986**, *55* (4), 1213−1223.
(55) Liang, L.; Meunier, V. *Nanoscale* **2014**, *6* (10), 5394−5401.
(56) Sugai, S.; Ueda, T.; Murase, K. *J. Phys. Soc. Jpn.* **1981**, *50* (10), 3356−3361.
(57) Ribeiro-Soares, J.; Almeida, R. M.; Cançado, L. G.; Dresselhaus, M. S.; Jorio, A. Group theory for structural analysis and lattice vibrations in phosphorene systems. 2015, *arXiv:1408.6641*. arXiv.org e-Print archive. http://arxiv.org/abs/1408.6641 (accessed April 2015).
(58) Ong, Z.-Y.; Cai, Y.; Zhang, G.; Zhang, Y.-W. *J. Phys. Chem. C* **2014**, *118* (43), 25272−25277.
(59) Ni, Z. H.; Wang, H. M.; Kasim, J.; Fan, H. M.; Yu, T.; Wu, Y. H.; Feng, Y. P.; Shen, Z. X. *Nano Lett.* **2007**, *7* (9), 2758−2763.
(60) Ribeiro, H. B.; Pimenta, M. A.; de Matos, C. J. S.; Moreira, R. L.; Rodin, A. S.; Zapata, J. D.; de Souza, E. A. T.; Castro Neto, A. H. *ACS Nano* **2015**, *9*, 4270−4276.
(61) Lu, W.; Nan, H.; Hong, J.; Chen, Y.; Zhu, C.; Liang, Z.; Ma, X.; Ni, Z.; Jin, C.; Zhang, Z. *Nano Res.* **2014**, *7* (6), 853−859.
(62) Yamamoto, M.; Wang, S. T.; Ni, M.; Lin, Y.-F.; Li, S.-L.; Aikawa, S.; Jian, W.-B.; Ueno, K.; Wakabayashi, K.; Tsukagoshi, K. *ACS Nano* **2014**, *8* (4), 3895−3903.
(63) Teweldebrhan, D.; Goyal, V.; Balandin, A. A. *Nano Lett.* **2010**, *10* (4), 1209−1218.
(64) Boukhicha, M.; Calandra, M.; Measson, M.-A.; Lancry, O.; Shukla, A. *Phys. Rev. B: Condens. Matter Mater. Phys.* **2013**, *87* (19), 195316.
(65) Klemens, P. G. *Phys. Rev.* **1966**, *148* (2), 845−848.
(66) Lin, J.; Guo, L.; Huang, Q.; Jia, Y.; Li, K.; Lai, X.; Chen, X. *Phys. Rev. B* **2011**, *83* (12), 125430.
(67) Calizo, I.; Balandin, A. A.; Bao, W.; Miao, F.; Lau, C. N. *Nano Lett.* **2007**, *7* (9), 2645−2649.
(68) Sahoo, S.; Gaur, A. P. S.; Ahmadi, M.; Guinel, M. J.-F.; Katiyar, R. S. *J. Phys. Chem. C* **2013**, *117* (17), 9042−9047.
(69) Lanzillo, N. A.; Birdwell, A. G.; Amani, M.; Crowne, F. J.; Shah, P. B.; Najmaei, S.; Liu, Z.; Ajayan, P. M.; Lou, J.; Dubey, M.; Nayak, S. K.; O'Regan, T. P. *Appl. Phys. Lett.* **2013**, *103* (9), 093102.
(70) Riedner, R. J.; Srinivasa, S. R.; Cartz, L.; Worlton, T. G.; Klinger, R.; Beyerlein, R. *ASCE* **1974**, *17*, 8−20.
(71) Raravikar, N. R.; Keblinski, P.; Rao, A. M.; Dresselhaus, M. S.; Schadler, L. S.; Ajayan, P. M. *Phys. Rev. B* **2002**, *66* (23), 235424.
(72) Kresse, G.; Furthmüller, J. *Comput. Mater. Sci.* **1996**, *6* (1), 15−50.
(73) Kresse, G.; Joubert, D. *Phys. Rev. B* **1999**, *59* (3), 1758−1775.
(74) Dai, J.; Zeng, X. C. *J. Phys. Chem. Lett.* **2014**, *5* (7), 1289−1293.
(75) Perdew, J. P.; Burke, K.; Ernzerhof, M. *Phys. Rev. Lett.* **1996**, *77* (18), 3865−3868.
(76) Grimme, S. *J. Comput. Chem.* **2006**, *27* (15), 1787−1799.
(77) Dion, M.; Rydberg, H.; Schröder, E.; Langreth, D. C.; Lundqvist, B. I. *Phys. Rev. Lett.* **2004**, *92* (24), 246401.
(78) Monkhorst, H. J.; Pack, J. D. *Phys. Rev. B* **1976**, *13* (12), 5188−5192.
(79) Liang, L.; Meunier, V. *Appl. Phys. Lett.* **2013**, *102* (14), 143101.